Wide-Field Imaging Interferometer Testbed Phase Retrieval

Alexander S. Iacchetta[a], James R. Fienup[a], David T. Leisawitz[b], Matthew R. Bolcar[b]
[a]Institute of Optics, Univ. of Rochester, 275 Hutchison Rd., Rochester, NY, USA 14627-0186
[b]NASA Goddard Space Flight Center, 8800 Greenbelt Rd., Greenbelt, MD, USA 20771-2400
Author e-mail address: alexander.iacchetta@rochester.edu

Abstract: We discuss the results of an experiment to recover system aberrations from Wide-field Imaging Interferometer Testbed (WIIT) images. We model the system with a unifying wavefront for all wavelengths, allowing slowly varying axial chromatic aberrations.
OCIS codes: (100.5070) Phase retrieval; (070.0070) Fourier optics and signal processing

1. Introduction to WIIT

The Wide-field Imaging Interferometer Testbed (WIIT) [1], including its calibrated hyperspectral image projector (CHIP) [2], at NASA's Goddard Space Flight Center is a state-of-the-art experimental realization of a dual-aperture wide-field spatio-spectral interferometer that operates at visible wavelengths. Spatio-spectral interferometry requires the collection of many images at different path delays between the arms of the interferometer, which is repeated for many different baseline separations and angles. The dataset is then reduced to a single hyperspectral image with a higher spatial resolution than that of the individual images of the dataset. In order to synthesize or simulate WIIT datasets, it is crucial to have knowledge of the optical system's aberrations and related point spread function (PSF) as a function of wavelength. We used CHIP and WIIT to perform an experiment to recover aberrations from the system's PSF.

Because WIIT's optical components that are non-common path are well-corrected flat mirrors with known surface profiles, we suspect that most of the system's aberrations are caused by an imaging lens after beam combination or by optical components before the entrance aperture of the interferometer. Knowing that the imaging lens is comprised of three achromatic doublets, it is likely that the system has axial chromatic aberrations that vary quadratically with wavelength. The isoplanatic patch size of the system is assumed to be at least as large as the full field-of-view of the image, which is supported in part by the fact that the imaging camera has a large f-number of about 80. For simplicity, we assume that the beams from both apertures overlap perfectly at the beam splitter and that the combined aperture is uniformly illuminated. Because the non-common path aberrations are small compared to the rest of the system's aberrations, we assume WIIT images derive from one underlying wavefront, modeled as having wavelength independent aberrations in addition to quadratically varying defocus. We now describe the measurements used to retrieve the wavefront through modern phase retrieval techniques [3, 4].

2. Phase Retrieval Measurements and Wavefront Model

The usable portion of CHIP's spectral response ranges from about 430 nm to 730 nm, peaking around 570 nm. CHIP's spatial engine is able to produce images at ten times the image resolution of WIIT's 16 micron camera pixels, so it is able to produce scenes that contain what are effectively point sources to WIIT's imaging camera. We used a spatial scene comprised of 5 well-separated, point-like sources, with one central source surrounded by 4 sources closer to the corners of the image plane. We took three sets of measurements with about 27 nm bandwidths centered on 475 nm, 575 nm, and 675 nm, where the detector was placed near the focus of the system as it would be during the system's normal mode of operation. A fourth set of measurements was taken with a 27 nm bandwidth centered on 575 nm, where the baseline length was increased to 230 mm in order to include the possibility that the projection mirror, which makes the scene appear to be in the far field of the interferometer's input aperture, has a significant impact on the system's aberrations.

Before performing phase retrieval, we preprocessed the data by first averaging 720 images of each scene and performing background subtraction, which is required because CHIP generates a spatially variant background pattern on top of which our scene is displayed. We then crop out all five PSFs in each image so that the resultant dataset has twenty images of 28x28 pixels each. Phase retrieval was then performed jointly on all twenty images.

We incorporated the assumptions mentioned in Sect.1 and made more simplifications to the phase retrieval problem. Our computational model initially allowed the tip/tilt and defocus terms of the wavefront to vary for each of the 20 PSFs, while all other higher-order aberrations were common to all of them. The unifying wavefront for the higher-order aberrations was described by Zernike polynomials through the 8^{th} radial order. Each individually modeled PSF had a 27 nm top-hat spectrum, where the defocus in microns, along with all other wavefront terms, was assumed to be constant over the entire 27 nm bandwidth.

Using the model described above where tip/tilt/defocus are independent variables for all 20 PSFs, we performed phase retrieval via nonlinear optimization of a bias-invariant error metric [3, 4], the square root of which is the normalized root mean-squared error (NRMSE) between the modeled PSFs and the measurements. We fit a quadratic to the retrieved defocus values as a function of wavelength and used that curve to compute new values for defocus at each of the 3 central wavelengths, effectively incorporating our assumption that the axial chromatic aberration has a quadratic shape. We then re-optimized the Zernike coefficients with the fixed defocus values.

3. Results and Conclusions

We found that, after the first round of optimization where defocus was freely varied for all 20 PSFs, the NRMSE was 0.0428. After fixing the defocus values to lie on the fitted curve and re-optimizing, the final NRMSE was 0.0437. Fig. 1(a) shows a plot of recovered peak-to-valley (PV) defocus values in microns and the curve that was fit to the data. The final wavefront without tip/tilt/defocus is shown in Fig. 1(b) with units of microns. Fig. 2 contains examples of modeled (top row) and measured (bottom row) PSFs for the on-axis sources, where the intensity values have been stretched to the 0.6 power after setting negative values to zero. There is particularly good agreement near the centers of the PSFs, and noise begins to dominate prior to reaching the inner edge of the red circles in Fig. 2.

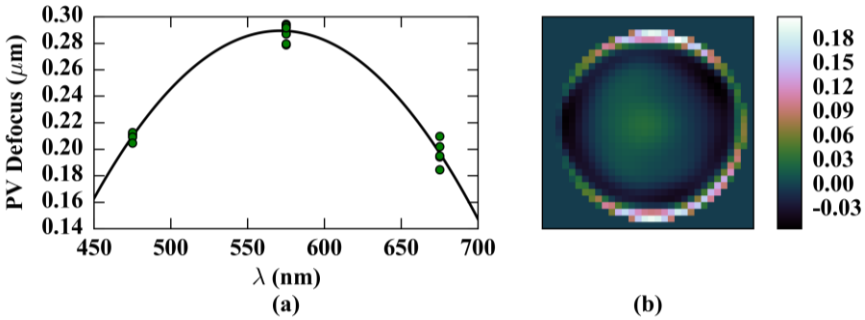

Fig. 1. Phase retrieval results. (a) Retrieved defocus in microns as a function of wavelength, and (b) all higher order aberration through 8th radial order Zernikes shown in microns.

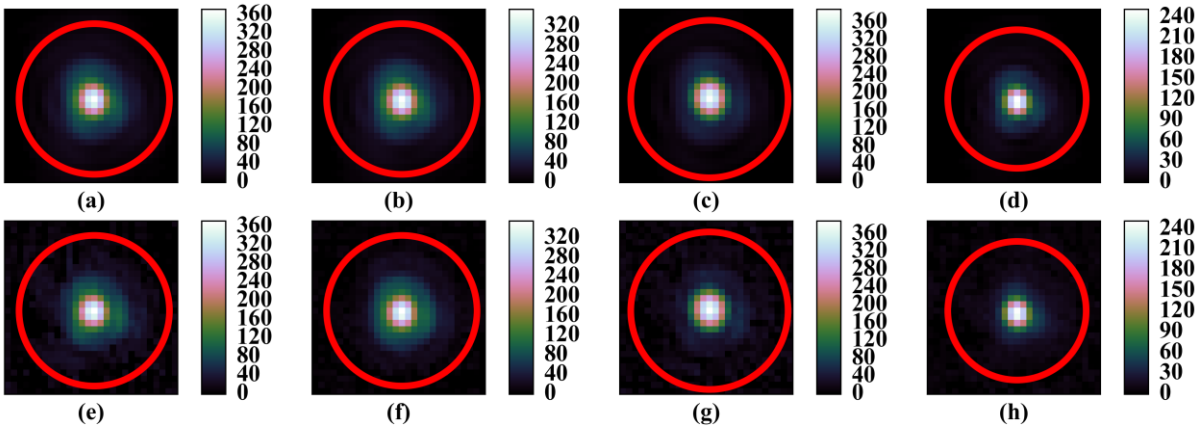

Fig. 2. (a–d) Modeled PSFs shown stretched to the 0.6 power after gain and bias adjustment, and (e–h) measured on-axis PSFs, where only pixels inside the red circles contributed to the optimizations. For (a, e) 575 nm source at 36 mm baseline, (b, f) 575 nm source at 230 mm baseline, (c, g) 675 nm source at 36 mm baseline, and (d, h) 475 nm source at 36 mm baseline. Note the colorbar shows stretched intensity values.

In conclusion, we have devised an experiment to recover aberrations that are representative of the WIIT system. We describe a simplified model for the system's aberrations and demonstrated that phase retrieval techniques can recover aberrations that agree with the measured data to within better than 4.5% on average. These results will allow for more accurate WIIT simulations, as well as provide the information needed to simultaneously synthesize and deconvolve WIIT datasets. This work was supported by a NASA Space Technology Research Fellowship.

4. References

[1] D. T. Leisawitz, M. R. Bolcar, R. G. Lyon, S. F. Maher, N. Memarsadeghi, S. A. Rinehart, and E. J. Sinukoff, "Developing wide-field spatio-spectral interferometry for far-infrared space applications," Proc. SPIE **8445**, 84450A (2012).

[2] M. R. Bolcar, D. T. Leisawitz, S. F. Maher, and S. A. Rinehart, "Demonstration of the Wide-field Imaging Interferometer Testbed using a Calibrated Hyperspectral Image Projector," Proc. SPIE **8445**, 84452D (2012).

[3] A.S. Jurling and J.R. Fienup, "Applications of Algorithmic Differentiation to Phase Retrieval Algorithms," JOSA A **31**, 1348-1359 (2014).

[4] S. T. Thurman and J. R. Fienup, "Phase retrieval with signal bias," JOSA A **26**, 1008-1014 (2009).